

Stochastic self-assembly of incommensurate clusters

M. R. D’Orsogna¹, G. Lakatos², and T. Chou³

¹*Dept. of Mathematics, CSUN, Los Angeles, CA 91330-8313*

²*Dept. of Chemistry, The University of British Columbia, Vancouver, BC, Canada, V6T-1Z1*

³*Depts. of Biomathematics and Mathematics, UCLA, Los Angeles, CA 90095-1766*

(Dated: May 24, 2022)

We examine the classic problem of homogeneous nucleation and growth by deriving and analyzing a fully discrete stochastic master equation. Upon comparison with results obtained from the corresponding mean-field Becker-Döring equations we find striking differences between the two corresponding equilibrium mean cluster concentrations. These discrepancies depend primarily on the divisibility of the total available mass by the maximum allowed cluster size, and the remainder. When such mass incommensurability arises, a single remainder particle can “emulsify” or “disperse” the system by significantly broadening the mean cluster size distribution. This finite-sized broadening effect is periodic in the total mass of the system and can arise even when the system size is asymptotically large, provided the ratio of the total mass to the maximum cluster size is finite. For such finite ratios we show that homogeneous nucleation in the limit of large, closed systems is not accurately described by classical mean-field mass-action approaches.

PACS numbers: 05.40.-a, 05.10.Gg, 64.75.Yz

Nucleation and growth arise in countless physical and biological settings [1]. In surface and material science, atoms and molecules may nucleate to form islands and multiphase structures that strongly affect overall material properties [2]. Nucleation and growth are also ubiquitous in cellular biology. The polymerization of actin filaments [3] and amyloid fibrils [4], the assembly of virus capsids [5] and of antimicrobial peptides into transmembrane pores [6], the recruitment of transcription factors, and the nucleation of clathrin-coated pits [7] are all important cell-level processes that can be cast as problems of nucleation and growth for which there is great interest in developing theoretical tools. Classical models of nucleation and growth include mass-action kinetics, such as the Becker-Döring (BD) equations describing the evolution of the *mean* concentrations of clusters of a given size [1], or models of independent clusters [8]. Solutions to the BD equations exhibit rich behavior, including metastable particle distributions [9], multiple time scales [10], and nontrivial convergence to equilibrium and coarsening [9, 11]. Within mean-field, mass-action treatments however, correlations, discreteness or stochastic effects are not included. These may be important, especially in applications to cell biology and nanotechnology, where small system sizes or finite cluster “stoichiometry” are involved.

In this paper, we carefully investigate the effects of discreteness and stochasticity for a simple, mass-conserving homogeneous nucleation process. We construct the *probability* of the system to be in a state with specified numbers of clusters of each size. A high-dimensional, fully stochastic master equation governing the evolution of the state probabilities is derived, simulated, and solved analytically in the equilibrium limit. Upon comparing the mean cluster concentrations found from the stochastic master equation with those obtained from the mean-field

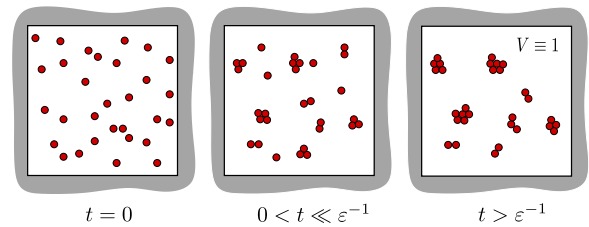


FIG. 1: (a) Homogeneous nucleation in a fixed, closed, unit volume initiated with $n_1(t=0) = M = 30$ monomers. For small detachment rates monomers will be nearly exhausted at long times. Here, the final cluster distribution consists of two dimers, one trimer, one 4-mer, one pentamer, and two hexamers.

BD equations, we find qualitative differences, even in the large system size limit. Our results highlight the importance of discreteness in nucleation and growth, and how its inclusion leads to dramatically different results from those obtained via classical, mean-field BD equations.

We begin by considering the simple homogeneous nucleation process in a closed system (Fig. 1). Monomers first bind together to form dimers. Larger clusters are formed by successive monomer binding but can also shrink by monomer detachment. Within cellular biophysics, nucleation and self-assembly often occur in small volumes. Here, monomer production/degradation may be slow compared to monomer attachment/detachment and the total number of monomers, both free and within clusters, can be assumed constant. Cluster sizes are also typically limited, either by the finite total mass of the system, or by some intrinsic stoichiometry. For example, virus capsids, clathrin coated pits, and antimicrobial peptide pores typically consist of $N \sim 100 - 1000$, $N \sim 10 - 20$, and $N \sim 5 - 8$ molecular subunits, respec-

tively. While various monomer binding and unbinding rate structures [9–12], cluster fragmentation/coagulation rules [13], or the presence of monomer sources [10, 14] can be included, for the sake of simplicity we consider only monomer binding and unbinding events occurring at constant, cluster size-independent rates.

Consider the probability density $P(\{n\}; t) \equiv P(n_1, n_2, \dots, n_N; t)$ of our system being in a state with n_1 monomers, n_2 dimers, n_3 trimers, \dots , n_N N -mers. The full stochastic master equation describing the time evolution of $P(\{n\}; t)$ is [14]

$$\begin{aligned} \dot{P}(\{n\}; t) = & -\Lambda(\{n\})P(\{n\}; t) \\ & + \frac{1}{2}(n_1 + 2)(n_1 + 1)W_1^+W_1^+W_2^-P(\{n\}; t) \\ & + \varepsilon(n_2 + 1)W_2^+W_1^-W_1^-P(\{n\}; t) \\ & + \sum_{i=2}^{N-1} (n_1 + 1)(n_i + 1)W_1^+W_i^+W_{i+1}^-P(\{n\}; t) \\ & + \varepsilon \sum_{i=3}^N (n_i + 1)W_1^-W_{i-1}^-W_i^+P(\{n\}; t). \quad (1) \end{aligned}$$

Here we non-dimensionalized time so that the binding rate is unity and the detachment rate is ε . Since it best illustrates the importance of discreteness in self-assembly, we henceforth restrict ourselves to the strong binding limit $\varepsilon \ll 1$. We define $\Lambda(\{n\}) = \frac{1}{2}n_1(n_1 - 1) + \sum_{i=2}^{N-1} n_1 n_i + \varepsilon \sum_{i=2}^N n_i$ as the total rate out of configuration $\{n\}$ and W_j^\pm as the unit raising/lowering operator that act the number of clusters of size j . For example, $W_1^+W_i^+W_{i+1}^-P(\{n\}; t) \equiv P(\{n'\}; t)$ where $\{n'\} = (n_1 + 1, \dots, n_i + 1, n_{i+1} - 1, \dots)$. We assume that all the mass is initially in the form of monomers: $P(\{n\}; t = 0) = \delta_{n_1, M} \delta_{n_2, 0} \dots \delta_{n_N, 0}$. By construction, the stochastic dynamics described by Eq. 1 obey the total mass conservation constraint $M = \sum_{k=1}^N k n_k$.

Solutions to Eq. 1 can be used to define quantities such as the mean numbers of clusters of size k : $\langle n_k(t) \rangle \equiv \sum_{\{n\}} n_k P(\{n\}; t)$. These mean numbers will be compared to the classical BD cluster concentrations $c_k(t)$ obtained by directly multiplying Eq. 1 by n_k and summing over all allowable configurations. This procedure leads to a hierarchy of equations relating the evolution of the mean $\langle n_k(t) \rangle$ to higher moments such as $\langle n_j(t) n_k(t) \rangle$. Closure of these equations using the mean-field and large number approximations, $\langle n_k n_j \rangle \simeq \langle n_k \rangle \langle n_j \rangle$ and $\langle n_1(n_1 - 1) \rangle \simeq \langle n_1 \rangle^2$, leads to the classical Becker-Döring equations

$$\begin{aligned} \dot{c}_1(t) &= -c_1^2 - c_1 \sum_{j=2}^{N-1} c_j + 2\varepsilon c_2 + \varepsilon \sum_{j=3}^N c_j \\ \dot{c}_2(t) &= -c_1 c_2 + \frac{1}{2} c_1^2 - \varepsilon c_2 + \varepsilon c_3 \\ \dot{c}_k(t) &= -c_1 c_k + c_1 c_{k-1} - \varepsilon c_k + \varepsilon c_{k+1} \\ \dot{c}_N(t) &= c_1 c_{N-1} - \varepsilon c_N, \end{aligned} \quad (2)$$

where $c_k(t)$ is the mass-action approximation to $\langle n_k(t) \rangle$. Here, the corresponding initial condition and mass conservation are expressed as $c_k(t = 0) = M \delta_{k,1}$ and $M = \sum_{k=1}^N k c_k(t)$, respectively. Eq. 2 can be easily integrated and analyzed at equilibrium in the $\varepsilon \ll 1$ limit

$$c_k^{\text{eq}} \approx \frac{\varepsilon}{2} \left(\frac{2M}{\varepsilon N} \right)^{k/N} \left[1 - \frac{k(N-1)}{N^2} \left(\frac{\varepsilon N}{2M} \right)^{1/N} + \dots \right].$$

where $c_k^{\text{eq}} \equiv c_k(t \rightarrow \infty)$. In equilibrium, mean-field BD theory predicts maximal clusters of size N dominate with concentration $c_N^{\text{eq}} \approx M/N$, while $c_{k < N}^{\text{eq}} \sim \varepsilon^{1-k/N} \approx 0$ as $\varepsilon \rightarrow 0^+$. Under mass-action thus nearly all the mass is driven into the largest cluster. However, a simple inconsistency emerges since the solution $c_k^{\text{eq}} \approx (M/N) \delta_{k,N}$ cannot be accurate if $M < N$, when there is insufficient mass to form a single maximal cluster.

To further investigate this inconsistency, we simulate the fully stochastic Master equation (1) using a KMC or residence time algorithm [15]. Figure 2 plots mean cluster numbers $\langle n_k(t) \rangle$ and mean-field results $c_k(t)$ with $N = 8$, $M = 16, 17$, and $\varepsilon = 10^{-6}$. Up to intermediate times $t \lesssim \varepsilon^{-1}$, there is little difference between the results for $M = 16$ and $M = 17$ and the mass-action concentrations $c_k(t)$ roughly approximate $\langle n_k(t) \rangle$. However, at long times $t \gg \varepsilon^{-1}$, striking differences arise between the $M = 2N = 16$ and $M = 2N + 1 = 17$ cases. We denote our solution in this limit as $\langle n_k^{\text{eq}} \rangle$, to be compared with c_k^{eq} . For the commensurate case $M = 16$ (Fig. 2(a)) the mass-action solution c_k^{eq} roughly approximates $\langle n_k^{\text{eq}} \rangle$, while for the incommensurate case $M = 17$, c_k^{eq} differs dramatically from $\langle n_k^{\text{eq}} \rangle$. Figure 2(c) highlights the differences between c_k^{eq} and $\langle n_k^{\text{eq}} \rangle$, particularly for $k = N = 8$ (red curves). The approximation $c_k^{\text{eq}} \sim \langle n_k^{\text{eq}} \rangle$ is reasonable only when M is exactly divisible by N , or, when M is very large. In the latter case, the periodically-varying mean cluster numbers $\langle n_N^{\text{eq}} \rangle \rightarrow c_N^{\text{eq}}$ as $M \rightarrow \infty$, while all other $\langle n_{k < N}^{\text{eq}} \rangle \rightarrow 0$.

To find analytic approximations to the equilibrium probabilities $P(\{n\}; t \rightarrow \infty)$, we make use of the fact that detachment is slow. In the $\varepsilon \ll 1$ limit, the most highly weighted equilibrium configurations are those with the fewest total number of clusters. For each set $\{M, N\}$, we can thus enumerate the states with the lowest number of clusters and use detailed balance to compute their relative weights. As an explicit example, consider the possible states for the simple case $N = 4$, $M = 9$ shown in Fig. 3. Here, nearly all the weight settles into states with the lowest number of clusters ($\mathcal{N}_{\min} = 3$ here). Applying detailed balance between the $\mathcal{N}_{\min} = 3$ and $\mathcal{N}_{\min} + 1 = 4$ states, neglecting corrections of $O(\varepsilon)$, we find $\langle n_1 \rangle \approx \langle n_2 \rangle \approx 6/13$, $\langle n_3 \rangle \approx 9/13$, and $\langle n_4 \rangle \approx 18/13$. This process can be extended to general M and N and leads to simple analytic solutions. Upon defining $M = \sigma N - j$ where σ denotes the maximum possible

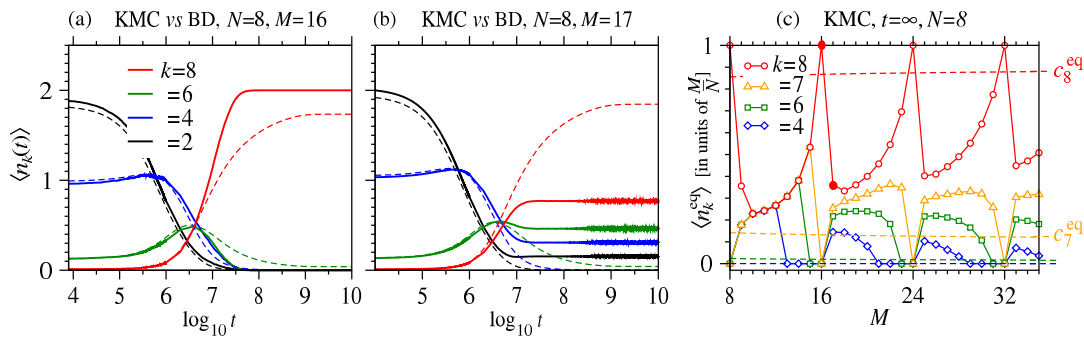


FIG. 2: Late-time mean cluster sizes $\langle n_k(t) \rangle$ obtained from averaging 10^6 KMC simulations of a stochastic nucleation process with $\varepsilon = 10^{-6}$. Only $k = 2, 4, 6, 8$ are displayed. (a) For $N = 8$ and $M = 16$, nearly all the mass is concentrated in $\langle n_8^{\text{eq}} \rangle \approx 2$ at equilibrium. (b) For $N = 8$, $M = 17$, a much broader equilibrium mean cluster distribution arises. For comparison, the numerical solution for $c_k(t)$ from the BD equations are displayed by the dashed curves. The simulation and mean-field results agree well with each other, but a dramatic difference arises at long times as equilibrium is approached, particularly when the total mass M is indivisible by N . (c) The difference between c_k^{eq} and $\langle n_k^{\text{eq}} \rangle$ (plotted in units of M/N) is highlighted as a function of M . The red dashed line corresponds to c_8^{eq} (which is nearly independent of M), while the open circles correspond to $\langle n_8^{\text{eq}} \rangle$ found from Monte-Carlo simulation. Note that $c_8^{\text{eq}} \sim \langle n_8^{\text{eq}} \rangle$ only when M is divisible by $N = 8$, or when $M/N \rightarrow \infty$. The filled red circles correspond to $M = 16$ and $M = 17$ as detailed in (a) and (b), respectively. A few other mean concentrations, $\langle n_{4,6,7}^{\text{eq}} \rangle$, along with the corresponding $c_{4,6,7}^{\text{eq}}$ (dashed lines) are also plotted for reference.

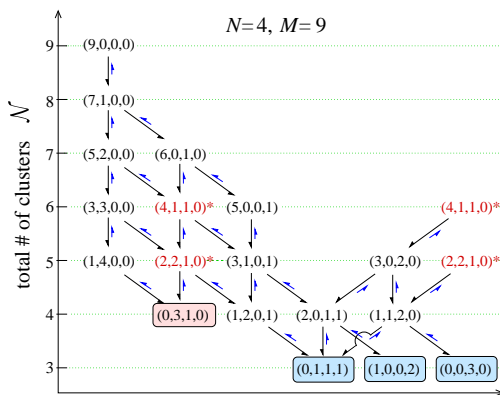


FIG. 3: Configurations (n_1, n_2, n_3, n_4) for $N = 4, M = 9$. Only three distinct states with a minimum number of clusters $\mathcal{N}_{\text{min}} = 3$ arise. These are all connected by monomer attachment/detachment events to states with $\mathcal{N}_{\text{min}} + 1 = 4$ clusters. Applying detailed balance between them leads to their weights in the $\varepsilon \rightarrow 0^+$ limit.

number of largest clusters, and $0 \leq j \leq N - 1$ represents the remainder of M/N , we arrive at one of our main results: exact solutions to the expected equilibrium cluster numbers in the $\varepsilon \rightarrow 0^+$ limit:

$$\langle n_N^{\text{eq}} \rangle = \frac{\sigma(\sigma - 1)}{(\sigma + j - 1)} \quad (3)$$

$$\langle n_{N-k}^{\text{eq}} \rangle = \frac{\sigma(\sigma - 1)j(j - 1) \dots (j - k + 1)}{(\sigma + j - 1)(\sigma + j - 2) \dots (\sigma + j - k - 1)}.$$

These expressions are valid for $0 \leq j < N - 1$ and all k . In the special case $j = N - 1$, the total mass can also

be expressed as $M = \sigma N - (N - 1) = (\sigma - 1)N + 1$ so that $j = N - 1$ corresponds to *adding* a single monomer to a system with $M = (\sigma - 1)N$ monomers. In this case, combinatoric factors of 2 that arise when monomers appear in the populated configurations must be taken into account leading to, for $j = N - 1$,

$$\langle n_1^{\text{eq}} \rangle = \frac{2(N - 1)!}{D(\sigma, N - 1)}$$

$$\langle n_{N-k}^{\text{eq}} \rangle = \frac{\prod_{\ell=1}^k (N - \ell) \prod_{i=1}^{N-k-1} (\sigma - 2 + i)}{D(\sigma, N - 1)} \quad (4)$$

$$\langle n_N^{\text{eq}} \rangle = (\sigma - 1) \frac{D(\sigma - 1, N - 1)}{D(\sigma, N - 1)},$$

where $D(\sigma, j) \equiv j! + \prod_{\ell=1}^{j-1} (\sigma + \ell)$. Eqs. 3 and 4 have been verified using extensive Monte-Carlo simulations.

Fig. 4 plots $\langle n_k^{\text{eq}} \rangle$ for $N = 8$ and varying M . Note that when $M = 16, 24, 32$ is divisible by $N = 8$ and $j = 0$, nearly all mass is deposited into the largest clusters, in agreement with the mass-action BD results. For cases where M is not an integer multiple of N and $j > 0$, there are remaining monomers that conspire to form smaller clusters. The number of ways this can happen may be large, generating a broad distribution of cluster sizes. For example, let us add a single monomer to the previously analyzed (Fig. 2(a)) state $N = 8, M = 16$ ($\sigma = 2, j = 0$). When $M = 17$ (Fig. 2(b)), Eq. 4 can be used by setting $\sigma = 3$ and $j = N - 1 = 7$. Note that by adding just a *single* monomer, the mean cluster size distribution which for $M = 16$ was concentrated into the largest cluster, disperses and nearly uniformly populates all cluster sizes. In our $N = 8, M = 17$ example, $(1, 0, 0, 0, 0, 0, 0, 2)$ is clearly one possible state with the lowest number of

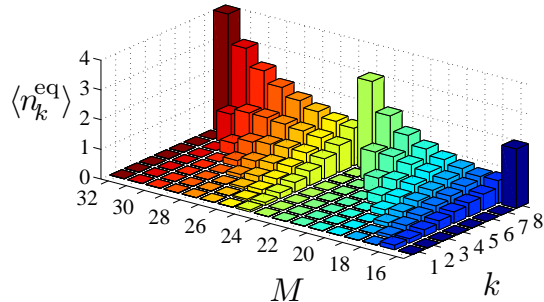


FIG. 4: The equilibrium cluster numbers $\langle n_k^{\text{eq}} \rangle$ as $\varepsilon \rightarrow 0^+$, plotted as functions of $1 \leq k \leq N = 8$ and M .

equilibrium cluster numbers ($\varepsilon \ll 1$)	$\frac{M}{N} \rightarrow 0$	$\frac{M}{N}$ finite	$\frac{M}{N} \gg N$
BD ($N = \infty$)	Eq. 2*	×	×
BD (finite N)	Eq. 2*	Eq. 2	Eq. 2†
stochastic model	Eq. 6*	Eqs. 6,7	Eqs. 6,7†

TABLE I: Accuracy and validity regimes for equilibrium cluster numbers of different nucleation models for $\varepsilon \ll 1$. Results indicated by * or by † match in the $\varepsilon \rightarrow 0^+$ limit, but approach their common result very differently in ε .

clusters $\mathcal{N}_{\min} = 3$. However, as long as some dissociation is allowed ($\varepsilon > 0$) a large number (in this case 7) of additional nontrivial 3-cluster states are possible: $(0, 1, 0, 0, 0, 0, 1, 1)$, $(0, 0, 0, 1, 0, 1, 1, 0)$, $(0, 0, 1, 0, 0, 1, 0, 1)$, $(0, 0, 0, 0, 2, 0, 1, 0)$, $(0, 0, 0, 1, 1, 0, 0, 1)$, $(0, 0, 1, 0, 0, 0, 2, 0)$, $(0, 0, 0, 0, 1, 2, 0, 0)$. The equilibrium weights of these 8 new states are comparable, resulting in a very flat mean cluster size distribution, if compared to the $N = 8, M = 16$ case.

We can quantify this “dispersal” effect by calculating the expected cluster values $\langle n_k^{\text{eq}} \rangle$ in the incommensurate cases using Eqs. 3 and 4. As shown in Figs. 4 and 2(c), when M gets large, the dispersal effect diminishes. Recall that the BD mass-action result $c_k^{\text{eq}} \sim (M/N)\delta_{k,N}$ puts all nearly all mass into c_N^{eq} , which is consistent with the exact solution in Eq. 4 only when $\langle n_{N-1}^{\text{eq}} \rangle / \langle n_N^{\text{eq}} \rangle \sim N^2/M \ll 1$. Thus, the mean-field result $c_k^{\text{eq}} \sim (M/N)\delta_{k,N}$ is asymptotically accurate only in the limit $M \gg N^2$, or equivalently, when $\sigma \gg N$. Thus, the periodically-varying curve $(N/M)\langle n_k^{\text{eq}} \rangle$ in Fig. 2(c) asymptotes to the mass-action result as $M/N^2 \rightarrow \infty$.

Finally, Table I lists regimes of validity and results for three different models: mass-action Becker-Döring equations without an imposed maximum cluster size, Becker-Döring equations with a fixed finite maximum cluster size N , and the fully stochastic master equation. Three dif-

ferent ways of taking the large system limits $M, N \rightarrow \infty$ are considered. The first column in Table I with $N = \infty$ and M finite corresponds to nucleation with unbounded cluster sizes. All models yield a single cluster of size M , but display different scaling behavior in ε (not discussed here). In the other extreme where $M/N \gg N$, equilibrium results from the finite- N BD equations match those of the discrete stochastic model and all the mass is concentrated into clusters of maximal size. However, just as before, the results from the mass-action and stochastic treatments approach their common distribution very differently in ε . The essential result described in our work applies in the intermediate case where M/N is finite, as summarized in the middle column of Table I. Here we find the novel incommensurability effect highlighted in Figs. 2(c) and 4. These effects persist even in the $M, N \rightarrow \infty$ limits, as long as their ratio is kept fixed. Our findings indicate that for many applications, where the effective M/N is finite, mean-field models of nucleation and growth fail and discrete stochastic treatments are required.

This work was supported by the NSF through grants DMS-1032131 (TC), DMS-1021818 (TC), DMS-0719462 (MD), and DMS-1021850 (MD). TC is also supported by the Army Research Office through grant 58386MA.

-
- [1] D. Kashchiev, *Nucleation: basic theory with applications*, (Butterworth-Heinemann, Oxford, 2000).
 - [2] J.G. Amar et al. *Mat. Res. Soc. Proc.* **570**, 3 (1999); M.N. Popescu et al. *Phys. Rev. B* **64**, 205404 (2001); P.A. Mulheran and M. Basham, *Phys. Rev. B* **77**, 075427 (2001).
 - [3] T.P.J. Knowles et al. *Science*, **326**, 1533 (2009); D. Sept and A.J. McCammon, *Biophys. J.*, **81**, 667 (2001); J. Miné et al. *Nucl. Acids Res.* **35**, 7171 (2007); L. Edelstein-Keshet and G. Ermentrout, *Bull. Math. Biol.* **60**, 449 (1998); M.F. Bishop and F.A. Ferrone, *Biophys. J.* **46**, 631 (1984).
 - [4] E.T. Powers and D.L. Powers, *Biophys. J.* **91**, 122 (2006).
 - [5] D. Endres and A. Zlotnick, *Biophys. J.* **83**, 1217 (2002); A. Zlotnick, *J. Mol. Biol.*, **366**, 14 (2007); B. Sweeney et al. *Biophys. J.* **94**, 772 (2008); J.Z. Porterfield and A. Zlotnick, An overview of capsid assembly kinetics, in *Emerging Topics in Physical Virology*, P. G. Stockley and R. Twarock (eds), (Imperial College Press, London, 2010), 131-158; A.Y. Morozov et al. *J. Chem. Phys.* **131**, 155101 (2009).
 - [6] K.A. Brogden, *Nat. Rev. Microbiol.* **3**, 238 (2005); G.L. Ryan and A.D. Rutenberg, *J. Bact.* **189**, 4749 (2007).
 - [7] M. Ehrlich et al. *Cell* **118**, 591 (2004). B.I. Shraiman, *Biophys. J.* **72**, 953 (1997); L. Foret and P. Sens, *Proc. Natl. Acad. Sci. USA* **105**, 14763 (2008).
 - [8] J. Kuipers and G. T. Barkema, *Phys. Rev. E*, **79**, 062101, (2009).
 - [9] O. Penrose, *J. Stat. Phys.* **89**, 305 (1997).
 - [10] J.A.D. Wattis and J.R. King, *J. Phys. A* **31**, 7169 (1998).

- [11] P.E. Jabin and B. Niethammer, *J. Diff. Equat.* **191**, 518 (2003); B. Niethammer, *J. Nonlin. Sci.* **13**, 115 (2008); T. Chou and M.R. D'Orsogna, *Phys. Rev. E* **84** 011608 (2011).
- [12] P. Smereka, *J. Stat. Phys.* **132**, 519 (2008).
- [13] S.N. Majumdar et al. *Phys. Rev. Lett.* **81**, 3691 (1998); *Statistical Physics of Irreversible Processes*, P.L. Krapivsky, E. Ben-Naim, and S. Redner, (Cambridge University Press, 2010).
- [14] J.S. Bhatt and I.J. Ford, *J. Chem. Phys.* **118**, 3166 (2003); F. Schweitzer et al. *Phys. A* **150**, 261 (1988).
- [15] A.B. Bortz et al. *J. Comp. Phys.* **17**, 10 (1975).